Multiphase equation of state of hydrogen from *ab initio* calculations in the range 0.2 to 5 g/cc up to 10 eV

L. Caillabet, S. Mazevet, and P. Loubeyre
CEA, DAM, DIF, F-91287 Arpajon, France

(Received 10 September 2010; revised manuscript received 15 December 2010; published 2 March 2011)

We construct a multiphase equation of state (EoS) of hydrogen in the range 0.2 to 5 g/cc and up to 10 eV based on *ab initio* electronic structure calculations. In the molecular solid, cold curve and phonon spectra calculations are performed for various structures, proposed in the literature, to cover the stability field up to 500 GPa. A weak structural dependence is observed, and the solid EoS is averaged over these data. In the dissociating molecular fluid and in the dense plasma, calculations are made to complete the abundant data set in the literature. Two physical models are used to fit these calculations: a double-Debye model for the solid phase and a one-component plasma model with a mass action law for dissociation to implicitly access the molecular phase in the fluid state. The output of the calculations; energy, pressure, temperature, and density are perfectly reproduced with thermodynamical consistency. This model also allows us to access to the total free energy. The ionic quantum zero-point contribution is taken into account. The present hydrogen EoS is shown to reproduce most of the existing experimental data very well: the solid compression curve, the Hugoniot curve, the sound velocity in the molecular fluid, and the melting curve. The usefulness of this EoS is illustrated by the computation of an interesting isotopic shift on the melting curve and of an isentropic compression path reaching temperatures lower than 1000 K in the terapascal range.

DOI: 10.1103/PhysRevB.83.094101 PACS number(s): 31.15.A−, 64.30.−t, 67.63.Cd

I. INTRODUCTION

The behavior of hydrogen at high pressures is the subject of intense study not only because the metallization of element one has remained elusive for the past 80 years, but also because it is a central input in various fields ranging from inertial confinement fusion (ICF) to the modeling of giant planets, such as Jupiter. The equation of state (EoS) is perhaps the most fundamental property to be determined. That is, the relation between the density, the pressure, and the temperature. In particular, a useful EoS should accurately span the extreme diversity of states of hydrogen, from the $T = 0$ K molecular solid, the atomic metal, the molecular fluid for the strongly degenerate plasma, as well as describe the transitions between them. Until now, the different EoSs of hydrogen used in applications are mostly based on chemical models, such as the SESAME,[1] the Saumon-Chabrier,[2] or the Ross ones.[3] They use physical models that are supposed to correctly describe the underlying physics and with enough independent parameters to adjust the EoS until it correctly reproduces the available experimental data. In the case of hydrogen, the EoS measurements remain scarce. The solid EoS has been accurately measured to 120 GPa at 300 K by single-crystal diffraction.[4] The dense fluid EoS has been measured along the principal Hugoniot up to 200 GPa using various approaches; gas gun,[5] Z pinch,[6] converging shocks,[7] and intense lasers,[8,9] now approaching good agreement.[10] On the other hand, *ab initio* calculations are proved to be an accurate approach to constrain the EoS of hydrogen over a large thermodynamical domain, out of experimental reach. In the past years, because of the enormous progress in computer capacity, first-principles calculations have been performed to compute, with good confidence, EoS data points for many systems.[11–13] Density functional theory (DFT) or full quantum Monte Carlo (QMC) simulations have already been performed for dense hydrogen.[14–24] These two calculations are specialized and are adapted to complementarily describe the various regions of the hydrogen phase diagram. The domain of validity of the DFT and QMC simulations has recently been discussed in the case of hydrogen.[24,25] Hence, a table of data points can be generated to reliably cover the EoS of hydrogen from the solid to the dense plasma.

It is the aim of this paper to build a thermodynamically consistent multiphase EoS of hydrogen adjusted on a complete grid of *ab initio* data points. As described later, this has been achieved in three steps. First, we have performed DFT calculations to constitute a complete set of data points, fully tested in terms of convergence, number of atoms, and numerical uncertainties. In principle, the only approximation of DFT calculations is the exchange-correlation functional. The GGA functional has been selected here because it brings good agreement with the solid experimental EoS. In the fluid state, numerous data points have already been published from DFT and from QMC simulations. These data are incorporated here. Our simulations complete these various calculations with special attention to the domain of the molecular dissociation. In the solid phase, DFT calculations of the 0-K isotherm and the phonon spectra have been performed for various structures. Second, as in the chemical approaches, we use physical models to fit the *ab initio* data set. In the solid phase, we employ a double-Debye model.[13] In the fluid phase, we use a one-component plasma model and a mass action law, with a fitted dissociation/ionization fraction to implicitly access the molecular phase. A quantum zero-point ionic contribution is also added. Such a parametrization allows obtaining an expression for the ionic entropy. Third, the present EoS is tested to reproduce all existing experimental data well.

The paper is organized as follows. In Sec. II, we describe the solid phase calculations and the fit with the double-Debye model. In Sec. III, the making up of the data set of the dense

fluid, from the molecular state to the plasma state, is explained and the associated free-energy model is described. The level of accuracy for the present EoS to reproduce all experimental data on hydrogen known so far is shown in Sec. IV. Two applications are discussed in Sec. V.

II. MOLECULAR SOLID

Following Chisolm *et al.*,[26] the total free energy in the solid phase, $F(V,T)$, is decomposed as the sum of three contributions,

$$F(V,T) = E_0(V) + F_e(V,T) + F_i(V,T), \quad (1)$$

where $E_0(V)$ is the electronic ground-state energy when the nuclei are fixed at their lattice sites, and where $F_e(V,T)$ and $F_i(V,T)$ are the electronic and ionic contributions, respectively. This decomposition assumes that the Born-Oppenheimer approximation is valid, thus, neglecting any contribution that may come from the electron-phonon interactions. Each contribution can be obtained directly using modern electronic structure calculations. This has recently been done by Correa *et al.*[13] for the construction of a fully *ab initio* EoS for carbon up to extreme pressures. Here, we follow a similar approach.

In the solid, we limit our investigation to the molecular phase. Correctly taking into account the quantum properties of the atomic phase is beyond the scope of this paper.[27] Also, it is shown later that the molecular phase should melt before it transforms into an atomic metal. The stability domain of the molecular solid phase has been estimated to extend up to at least 500 GPa, either by extrapolating experimental data[4] or by using the most recent calculations.[16] Up to 300 GPa, at least three different phases have been observed for molecular hydrogen. Phase I is an hcp structure with freely rotating molecules.[4,28] Phases II and III are associated with quantum and classical ordering, respectively, of the molecules.[29] Phase II is a purely orientational transition on the hcp lattice with a local order giving incommensurate modulation of the structure.[30] The volume discontinuity at the transition is very small. The nature of phase III is still unknown but should be obtained through a displacive path from phases I and II. Numerous *ab initio* calculations[16,31–34] have tried to identify the structural changes of hydrogen under pressure, but so far, no definite answer has emerged. This uncertainty is in part due to the small enthalpy difference between the various possible phases and also to subtle quantum effects that might influence the answer, such as the quantum rotational state of the molecules, which is beyond standard DFT modeling.

From the viewpoint of constructing an EoS, the aim is not to determine the most stable structure but to show that the EoS has a weak sensitivity on the detailed nature of the best candidate structures. Also, in the theoretical framework given by Eq. (1), it is important to consider structures as dynamically stable so as to calculate the ionic contribution to the free energy, $F_i(V,T)$. Consequently, we calculated the EoS of solid molecular hydrogen using four different structures that represent the diversity of possible structures so as to quantify the sensitivity of the EoS to the structural uncertainty. More specifically: We consider the m-hcp structure where the centers of the molecules form an hcp lattice with a fixed molecular orientation along the c axis; the orthorhombic $Pca2_1$ structure with eight atoms per unit cell, which has been proposed as a probable candidate for phase II;[31,32,34,35] the Pa3 structure, observed for a metastable solid of ortho-H_2 at low temperatures where the center of the molecules form an fcc lattice and their axes are oriented along the body diagonal of the cube;[36] and the orthorhombic Cmca structure with eight atoms per unit cell, which has been proposed as the structure of phase III.[16,33]

TABLE I. Vinet fit parameters of the electronic ground-state energy $E_0(V)$, for various structures and using two approximations for the exchange-correlation functional, LDA or GGA.

	$E_0(0)$ eV/atm	V_0 cc/mol	K_0 GPa	K_0' GPa
Pa3 LDA	−15.534	10.98	2.10	6.04
Pa3 GGA	−15.884	19.24	0.22	7.29
$Pca2_1$ GGA	−15.878	20.92	0.17	7.34
m-hcp GGA	−15.882	19.85	0.16	6.81
Cmca GGA	−15.680	39.59	0.0047	9.60

To perform the electronic structure calculations, we used the ABINIT electronic structure code[37] and a Trouiller-Martin pseudopotential with a cutoff radius of $0.6a_B$ to reach the highest pressure.[38] The cutoff energy was set to 240 hartree, while the **k**-points sampling was varied from 6^3 for the Pa3 structure to 14^3 for the Cmca structure. We used the Perdew-Burke-Ernzerhof exchange-correlation functional[39] in the generalized gradient approximation (GGA) of the DFT and the Ceperley-Alder functional[40] for the local-density approximation (LDA). For each density, the ionic positions and, subsequently, the lattice parameters have been relaxed in the three directions at fixed volume.

The ground-state energy $E_0(V)$, calculated for the four considered structures, is fitted by a Vinet form.[41] A Vinet form provides a simple parametrization of an EoS and expresses the energy variation as a function of volume as

$$E_0(X) = E_0(0) + \frac{4V_0K_0}{(K_0'-1)^2}\left\{1 - \left[1 - \frac{3}{2}(K_0'-1)(1-X^{1/3})\right] \times \exp\left[\frac{3}{2}(K_0'-1)(1-X^{1/3})\right]\right\}, \quad (2)$$

where X is the reduced volume that is defined as $X = V/V_0$, with V_0 as the equilibrium volume. The bulk modulus is expressed as $K_0 = -V(\frac{\partial P}{\partial V})_0$ and $K_0' = \frac{\partial K_0}{\partial P}$. The four parameters of the Vinet form are given in Table I for each structure. We see that the equilibrium volumes and bulk moduli obtained are rather close for the Pa3, the $Pca2_1$, and the m-hcp structures, but significant deviations are noticeable in the case of Cmca. The difference can be traced back to the difficulty of relaxing the Cmca structure around its equilibrium volume because this structure is only mechanically stable at high pressure.[16] Indeed, above 150 GPa, the energy and pressure of the Cmca structure become rather close to the values of the other three structures, despite the apparent difference of the fit parameters shown in Table I. On the other hand, a significant difference is observed between the LDA or the GGA approximations. As shown by a recent systematic study

on transition metals,[12] the comparison between the calculated and experimental EoS is a good test of the approximation used for the exchange-correlation functional. It will be shown in the following that the GGA approximation offers a much better description of the hydrogen EoS than the LDA. The values obtained for the equilibrium volumes also appear rather far from the experimental value $V_{\rm exp} = 23.00$ cc/mol.[42] These are, however, obtained without taking into account either the contribution from the zero-point motion (ZPM) of the ions or the dispersion forces that are not calculated correctly by the DFT. The ZPM of the nuclei is large enough to significantly affect the equilibrium volume of the various hydrogen isotopes and, indeed, the calculated values around 20.00 cc/mol are closer to the D_2 equilibrium volume $V_{\rm exp} = 19.93$ cc/mol,[43] for which the ZPM contribution is much smaller. That ionic quantum effect will be taken fully into account later by calculating the ionic contribution to the free energy using linear response theory and a double-Debye model fit of the phonon spectra.

To obtain the phonon dispersion curves shown in Fig. 1, we performed linear response calculations on the relaxed structure found at a given volume. We used the approach implemented in the ABINIT code based on density functional perturbation theory (DFPT).[44] In this method, the coefficients of the dynamic matrix in reciprocal space are proportional to the second derivative of the energy with respect to the atomic displacements. The same numerical approximations, as described previously for the energy calculation, have been used. They give frequencies convergence to better than 0.04 THz over the whole phonon dispersion curves. We paid particular attention to the stability domain for each structure.

Phonon calculations have been performed for the Pa3, the $Pca2_1$, and the Cmca structures. The m-hcp structure is found mechanically unstable up to at least 150 GPa and so was not considered for estimating the ionic free-energy contribution. As shown in Fig. 1, an increase in pressure leads to the appearance of an imaginary transverse acoustic mode in the $M \rightarrow \Gamma$ direction for the Pa3 structure and in the $X \rightarrow U$ direction for the $Pca2_1$ structure. This gives us an upper limit for the stability of these two structures, up to 191 GPa for the Pa3 structure and 158 GPa for the $Pca2_1$. This imaginary mode is present in both the LDA and the GGA descriptions, but it appears at lower pressure, $P = 136$ GPa, when the LDA functional is used. These results for the $Pca2_1$ structure are similar to those obtained by Zhang *et al.*[45] with a soft mode located at the **X** point (we note that Zhang *et al.* locate the soft mode at the **Y** point for the $Pca2_1$ phase. The spectra being identical otherwise, we attribute this difference to a simple mislabeling in the paper). The Cmca phonon spectra are only calculated in the stability domain of phase III, for which they are a good candidate structure. They are found to be stable from 150 GPa to at least 500 GPa in the GGA approximation. Here, the important point is that the stability domain of these various structures overlap. So, the ionic free-energy contribution of Eq. (1) can be estimated over the whole stability domain of the molecular solid phase.

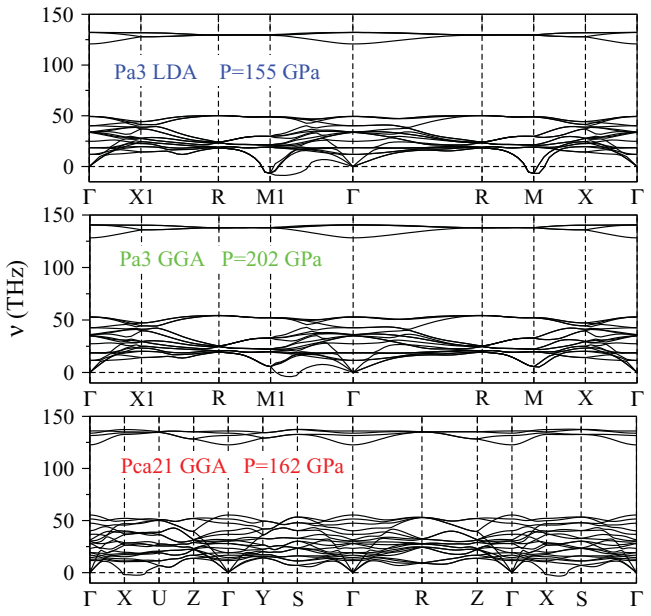

FIG. 1. (Color online) Typical phonon dispersion spectra indicating the mechanical instability of the Pa3 and Pca21 structures at high pressure.

From the phonon spectra calculated using linear response theory, the ionic contribution to the free energy can be obtained directly within the framework of the quasiharmonic approximation, as given by[46]

$$F_{\rm ph}(V,T) = \int_0^\infty g(\omega)\left[\frac{1}{2}\hbar\omega + \beta^{-1}\,\ln\left(1 - e^{-\beta\hbar\omega}\right)\right] d\omega. \quad (3)$$

In Eq. (3), $g(\omega)$ represents the phonon density of state (PDOS) at a given volume V and is the direct outcome of DFPT calculations.

Figure 2 shows the typical PDOS for the three structures considered. These calculated PDOSs present a double peak structure that is rather different from the usual Debye form. The high-frequency region can be associated with the vibron modes at around 4000 $\rm cm^{-1}$. The lower-frequency domain is associated with libron and phonon modes with frequencies centered around 1000 $\rm cm^{-1}$. Following Correa *et al.*, we employ a double-Debye model, in which the PDOS is approximated by two overlapping Debye peaks, each of which is characterized by its own volume-dependent Debye temperature. Thus, the calculated PDOS is fitted by a linear combination of two Debye density of states given by

$$g_V(\omega) = \xi_V^A g_V^A(\omega) + \xi_V^B g_V^B(\omega), \quad (4)$$

g_V^A and g_V^B are equal to $3\omega^2/\omega_D^3$ for $\omega < \omega_D$ and zero otherwise. The coefficients ξ_V^A and ξ_V^B are calculated at each volume where a phonon calculation is performed. They are obtained by imposing the normalization condition $\xi_V^A + \xi_V^B = 1$ and requiring that the three phonon moments, θ_0, θ_1, and θ_2 are equal to those computed from the true PDOS at each volume:

$$\begin{aligned} \ln(\theta_0) &= \xi_V^A\,\ln(\theta_A) + \xi_V^B\,\ln(\theta_B), \\ \theta_1 &= \xi_V^A\theta_A + \xi_V^B\theta_B, \\ \theta_2 &= \xi_V^A\theta_A^2 + \xi_V^B\theta_B^2. \end{aligned} \quad (5)$$

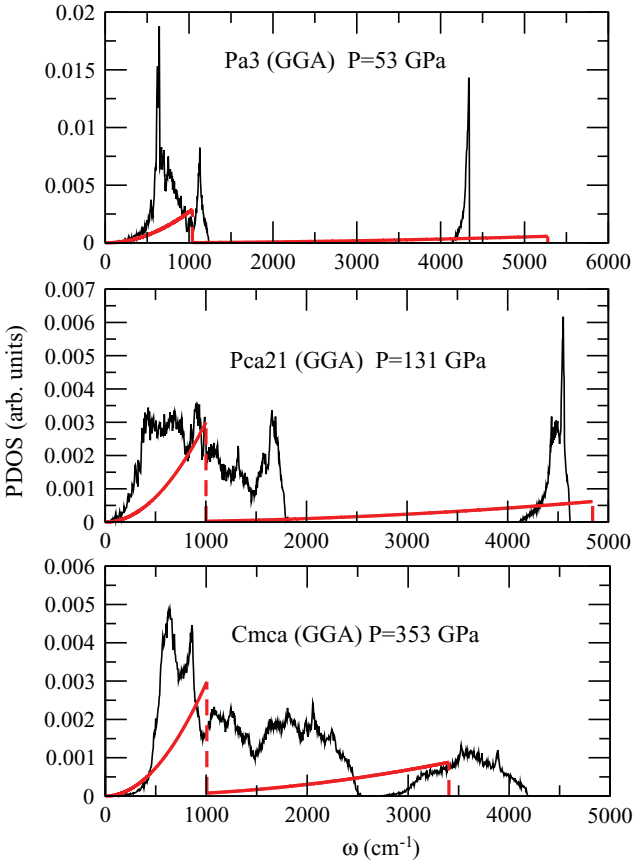

FIG. 2. (Color online) Phonon density of state for the Pa3, the $Pca2_1$, and the Cmca structures at representative pressures, in black, and comparison to their representation by a double-Debye model, in red (see text).

In Eq. (5), θ_A and θ_B, respectively, are the Debye temperatures corresponding to the density of state g_V^A and g_V^B. The moments θ_0, θ_1, and θ_2 are defined as[26]

$$k_B\theta_0(V) = \hbar e^{1/3} \exp\left(\int \log(\omega) g_V(\omega)\, d\omega\right),$$
$$k_B\theta_1(V) = \frac{4}{3}\int \hbar\omega g_V(\omega)\, d\omega, \tag{6}$$
$$k_B\theta_2(V) = \left(\frac{5}{3}\int (\hbar\omega)^2 g_V(\omega)\, d\omega\right)^{1/2}. \tag{7}$$

In this formulation, the zero-point motion contribution to the free energy is given by $F_{\rm ph}(V,T) = \frac{9}{8}k_B\theta_1$. Following Correa, one further imposes $\theta_A \leqslant \theta_B$ with $\xi_V^A = \frac{\ln(\theta_B/\theta_0)}{\ln(\theta_B/\theta_A)}$ and $\xi_V^B = \frac{\ln(\theta_0/\theta_A)}{\ln(\theta_B/\theta_A)}$. Finally, the V dependence of the Debye temperatures θ_A and θ_B is taken into account by assuming that their respective Grüneisen parameters ($\gamma_{A,B,0}$) vary linearly with volume,

$$-\frac{d\,\ln(\theta_{\{0,A,B\}})}{d\,\ln(V)} = \gamma_{\{0,A,B\}}(V) \tag{8}$$
$$= \alpha_{\{0,A,B\}} + \beta_{\{0,A,B\}}\,\ln(V). \tag{9}$$

The parameters of the double-Debye model fitting to the PDOS of the three structures considered are given in Table II.

For the present scope of the paper, the selection criteria for the double-Debye fit is how accurately they represent the ionic contribution to the free energy. The ionic contribution to the free energy is expressed as

$$F_h(V,T) = \xi_V^A f_h^A(V,T) + \xi_V^B f_h^B(V,T), \tag{10}$$

where $f_h^B(V,T)$ and $\mathcal{D}(y)$ are given by

$$f_h^{A,B} = k_B T\left\{\frac{9}{8}\frac{\theta_{A,B}}{T} + 3\ln[1-e^{-\theta_{A,B}/T}] - \mathcal{D}\left(\frac{\theta_{A,B}}{T}\right)\right\},$$
$$\mathcal{D}(y) = \frac{3}{y^3}\int_0^y \frac{x^3}{\exp(x)-1}dx. \tag{11}$$

In Fig. 3, the ionic contribution to the free energy calculated from the *ab initio* PDOS and from the double-Debye model are compared. They agree to better than 5×10^{-3} eV/atom for each structure. Thus, the double-Debye model is extremely well suited for modeling the ionic contribution to the free energy of molecular solid hydrogen. It should be noted that the electronic contribution to the free energy, as given by $F_e(V,T)$ in Eq. (1) is calculated to be extremely small in the stability domain of the molecular phase, i.e., for temperatures below 0.2 eV. Thus, it is neglected.

Using the parametrization of the electronic ground-state energy and that of the ionic free energy, the EoS is calculated at $T = 300$ K for the Pa3 and the $Pca2_1$ structures. In Fig. 4, these EoSs are compared to the experimental data[47] (corrected with the new high-pressure scale[12]). The difference between the various structures is smaller than the difference obtained by using different functionals, GGA or LDA. Good agreement with the experiment is obtained with the GGA approximation. Consequently, we construct the EoS of molecular solid hydrogen up to 500 GPa using the GGA-DFT calculations described earlier for the m-hcp, the Pa3, the $Pca2_1$, and the Cmca structures. For the cold curve contribution, $E_0(V)$, a Vinet form is fitted to the combined data sets calculated for the m-hcp, the Pa_3, the $Pca2_1$, and the Cmca structures. For the ionic contribution, the parameters of the double-Debye model are obtained by a mean-square adjustment of the phonon moments, θ_0, θ_1, and θ_2 calculated

TABLE II. Parameters of the double-Debye model fit obtained for various structures, Pa3, Pca21, Cmca, and two functionals, LDA and GGA. The domain over which the fit has been performed is indicated.

	$\theta_{\{0\}}^{(0)}$ (K)	$\alpha_{\{0\}}$	$\beta_{\{0\}}$	$\theta_{\{A\}}^{(0)}$ (K)	$\alpha_{\{A\}}$	$\beta_{\{A\}}$	$\theta_{\{B\}}^{(0)}$ (K)	$\alpha_{\{B\}}$	$\beta_{\{B\}}$	Range
Pa3 LDA	2810.45	0.089	0.454	1757.24	−0.128	0.661	6792.67	−0.046	0.018	$0 \leqslant P \leqslant 136$ GPa
Pa3 GGA	3147.61	0.162	0.308	2078.50	−0.079	0.543	7151.66	−0.099	0.082	$0 \leqslant P \leqslant 191$ GPa
$Pca2_1$ GGA	3141.01	0.286	0.310	1874.32	0.094	0.481	6188.82	−0.185	0.083	$0 \leqslant P \leqslant 158$ GPa
Cmca GGA	3973.49	1.108	−1.266	4367.74	4.436	−8.871	7318.06	1.809	−3.997	$180 \leqslant P \leqslant 533$ GPa

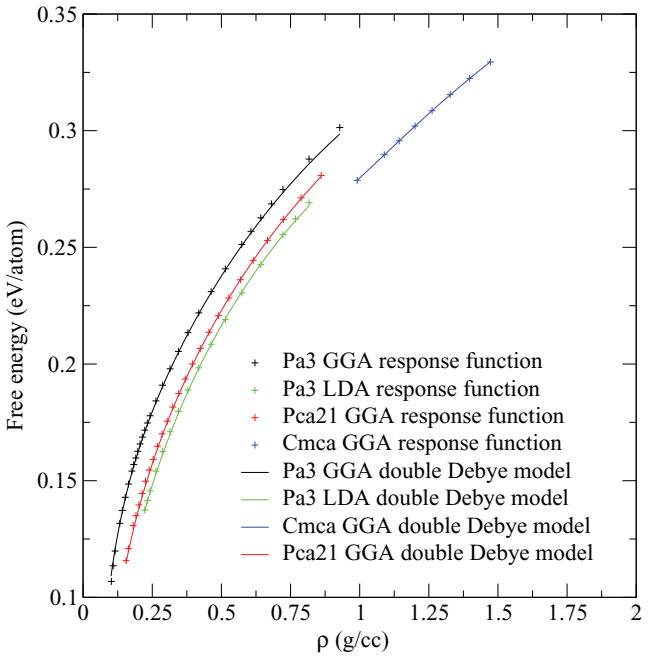

FIG. 3. (Color online) Ionic contribution to the solid free energy in various structures: calculations from the *ab initio* PDOS, as data points, and their fit by a double-Debye model, as full lines.

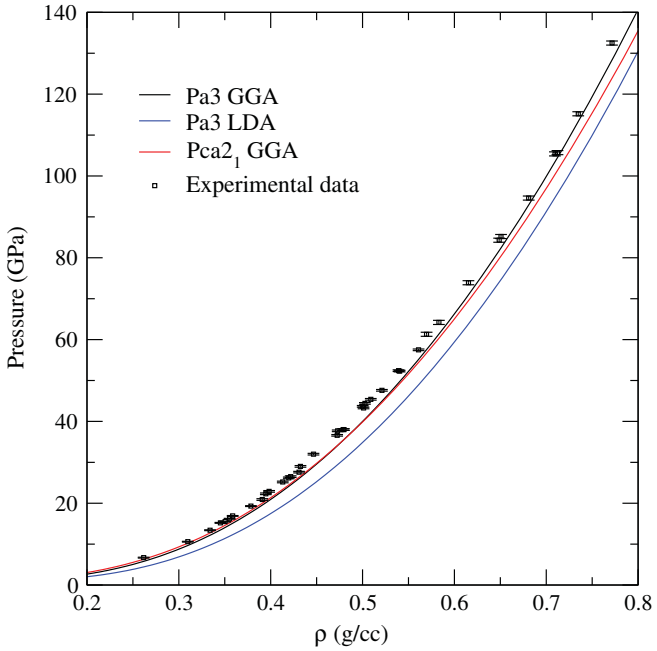

FIG. 4. (Color online) Comparison between the $T = 300$ K isotherm for the Pa3 (GGA and LDA) and $Pca2_1$ (GGA) structures and the experimental data[4] corrected for the pressure scale.[12]

for the three structures, Pa_3, $Pca2_1$, and Cmca, at various pressures over ranges given in Table II. The parameters of these fits are given in Table III. It is seen that a 12-parameter EoS can describe the *ab initio*-based EoS of molecular solid hydrogen up to 500 GPa. Figure 5 shows the resulting 300-K isotherm obtained using this structure-independent molecular solid EoS compared to the 300-K isotherm obtained when considering each structure separately. The solid EoS indeed averages the EoS of the various structures. In the inset, it is compared to the experimental $T = 300$ K X-ray data,[4] and the agreement is satisfactory. At present, it is impossible to determine whether the small difference is due to the built-in structural uncertainty or the approximations made in the GGA functional.

III. LIQUID AND PLASMA STATES

Over the past ten years, a large amount of work has been devoted to calculating the thermodynamics properties of warm dense hydrogen using *ab initio* methods. This theoretical effort has been spurred by a significant experimental extension of the deuterium Hugoniot by laser-shock measurements, showing a maximum compression ratio of about 6,[8] whereas, *ab initio* calculations were predicting a ratio closer to 4.5.[17] Over the same period, the experimental determination of the Hugoniot has been revisited by many groups and various techniques. Now, it seems that an experimental consensus is emerging for a maximum compression ratio along the experimental hydrogen Hugoniot around 4.5.[9,10] This agreement achieved between calculations and experiments along the Hugoniot of hydrogen is bringing some confidence to the adequacy of *ab initio* approaches for describing dense hydrogen. Furthermore, the comparison between these various calculations based on different approximations has provided a better view on the range of applicability of each approach. Path integral Monte Carlo (PIMC) is accurate at very high temperatures (above 20 000 K), whereas, for intermediate temperatures and high pressures, the DFT molecular dynamics [quantum molecular dynamics (QMD)] is the best adapted computational method.[19,24] A large body of calculations on the EoS of warm dense hydrogen exists in the literature.[20,21,23,24,48] Here, we gather a selection of three *ab initio* EoS calculations in the dense fluid, specifically: the QMD simulations, extended and fitted by Holst *et al.*,[23] which span in densities from 0.2c to 5 g/cc for temperatures between 500 and 20 000 K; the coupled electron-ion Monte Carlo(CEIMC) results of Morales *et al.*,[24] which provide a parametrization of the free energy of the atomic liquid for densities between 0.7 and 2.4 g/cc and temperatures between 2000 and 10 000 K; and the PIMC calculations[19] above 20 000 K and up to 125 000 K at various densities between 0.195 and 2.695 g/cc.

TABLE III. Full parametrization of the *ab initio*-based solid molecular hydrogen EoS.

$E_0(V)$				$F_i(V,T)$								
$E_0(0)$	V_0	K_0	K_0'	$\theta^{(0)}_{\{0\}}$	$\alpha_{\{0\}}$	$\beta_{\{0\}}$	$\theta^{(0)}_{\{A\}}$	$\alpha_{\{A\}}$	$\beta_{\{A\}}$	$\theta^{(0)}_{\{B\}}$	$\alpha_{\{B\}}$	$\beta_{\{B\}}$
−15.878	20.58	0.16	7.42	3609.41	0.457	0.146	1434.97	−0.253	0.599	4348.99	−0.622	0.336

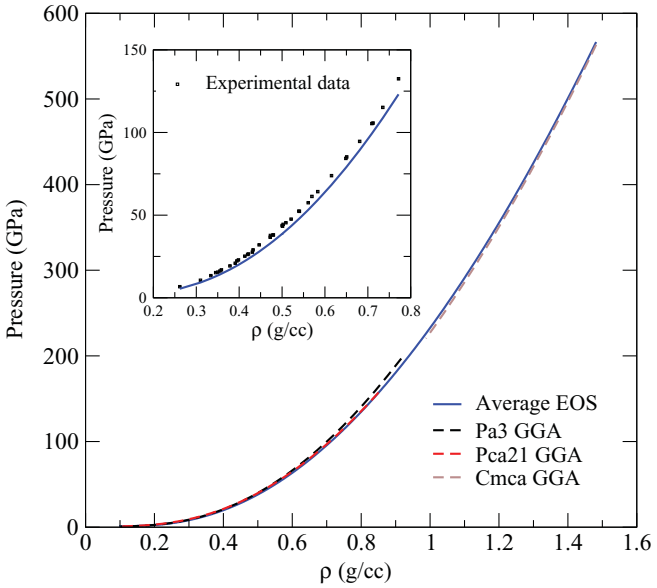

FIG. 5. (Color online) Comparison between the 300-K solid EoS and those of various structures. Inset: relative difference between the solid EoS and the experimental data of Ref. 4 (corrected for the new high-pressure scale[12]).

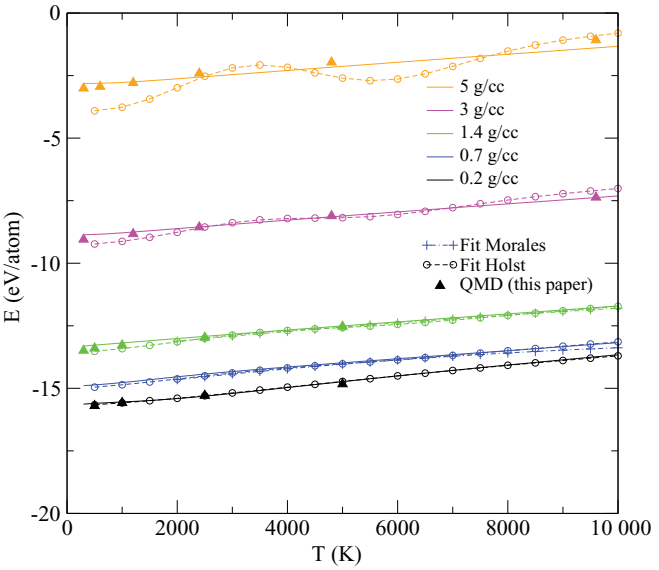

FIG. 6. (Color online) Variation of the internal energy versus temperature for various densities: the present QMD simulation data; the fitted QMD calculations of Holst *et al.*;[23] the fitted CEIMC calculations of Morales *et al.*[24] The full line is the present *ab initio*-based EoS.

These three *ab initio* data sets have been supplemented by some *ab initio* simulations to quantify possible uncertainties arising from the fits used to represent the published data. Simulations have been performed in the NVT (canonical) ensemble where the number of particles and the volume are fixed, while a simple velocity scaling is applied to maintain the ion temperature constant. A plane-wave cutoff of 240 hartree was necessary to obtain convergence for the pressure and for the internal energy to better than 1%. We performed the simulations using 144 atoms in the simulation cell and a $2 \times 2 \times 2$ **k**-point grid as given in the Monkhorst-Pack scheme. We checked that these simulation parameters were optimized by increasing the number of atoms to 512 for a few representative points. The present set of data points, covering the range 0.2 to 5 g/cc over the temperature domain 300–10 000 K, is plotted in Fig. 6. Very good agreement between our QMD simulations data and the fitted QMD results of Holst *et al.*[23] by a density expansion is observed below 1.4 g/cc. However, Holst's *et al.* parametrization seems to generate some unphysical oscillations at higher densities. Very good agreement is also obtained between our data and the CEIMC calculations.

A. Parametrization of the free energy

There is no universally applicable model, such as the Debye model for the solid, to describe the free energy of a fluid or a plasma. However, the free-energy form of a plasma, even strongly coupled and degenerate, is well documented in the literature. The free energy can be written as the sum of three terms,

$$F = F_{id}^{(i)} + F_{id}^{(e)} + F_{ex}, \tag{12}$$

where $F_{id}^{(i)}$ and $F_{id}^{(e)}$, respectively, denote the ideal free energy of the ions and electrons (including entropy of spin) and F_{ex} is the excess free energy arising from Coulombic interactions. The H plasma is essentially characterized by the density parameter $r_s = a_e/a_0$, where a_0 is the Bohr radius, $a_e = (\frac{4}{3}\pi n_e)^{-1/3}$ is the electron sphere radius, n_e is the electron density, and $\Gamma = (e)^2/a_i k_B T$ is the Coulomb coupling parameter, where a_i is the ionic sphere radius. In the case of hydrogen, $a_i = a_e$. Chabrier and Potekhin[49] have proposed an analytic form for F_{ex}, which should be valid at any temperature for a fully ionized plasma since the attractive Coulombic interaction per electron is very weak compared to the Fermi energy. In this case, the ion-electron interaction can be treated within the linear screening theory,[50] and thus, F_{ex} can be separated in three terms:

$$F_{ex} = F_{ii} + F_{ie} + F_{ee}. \tag{13}$$

The free energy of ion-ion interaction F_{ii} is described by the standard DeWitt-Slattery-Chabrier model (DWSC),[51] particularly suitable for $1 \leqslant \Gamma \leqslant 160$. The free energy of electron-electron interaction F_{ee} is given by the Ichimaru, Iyetomi, and Tanaka formula (IIT)[52]. The linear-response treatment of the ion-electron interaction is suitable at large densities due to the weak electronic polarization by the ionic charge distribution, and Kohanoff and Hansen[53] have shown that it becomes rapidly unreliable at densities below 20 g/cc for hydrogen. Indeed, as the density decreases, the electron gas becomes more and more polarized because of its strong inhomogeneity, especially in the domain of strong degeneracy (i.e., $T \ll T_F$). However, as the temperature increases, the polarizability of the electron gas decreases, and the effective interionic potential becomes indistinguishable from a Yukawa potential at $T \sim T_F$.[54] For the lowest density (0.2 g/cc) of our domain of study, $T_F \sim 100\,000$ K. So, as long as $T \geqslant 100\,000$ K, the model of Chabrier and Potekhin should be suitable in the range of density considered here. Indeed, we

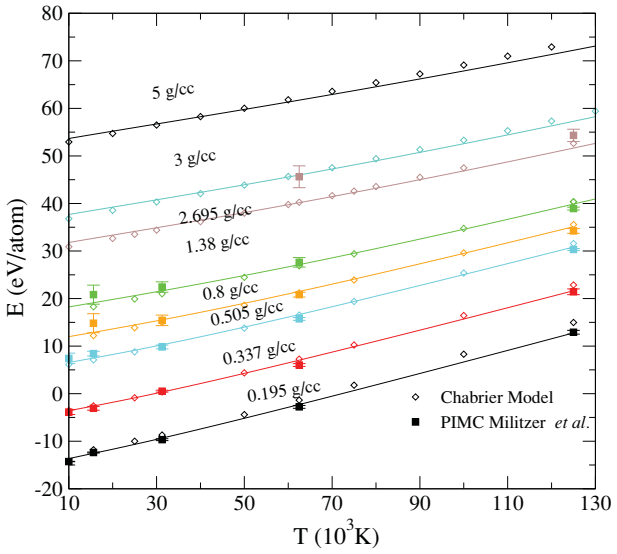

FIG. 7. (Color online) Internal energy versus temperature above 10 000 K at various densities obtained using the PIMC calculation,[19] a fully ionized dense plasma model,[49,55] and the present *ab initio*-based EoS. Each curve corresponds to an isochore. Each curve has been shifted by 5 eV from the previous one for clarity.

can see in Fig. 7 that the internal energy given by this model is in good agreement with PIMC calculations in the 100 000-K range for the lowest densities, and this agreement extends toward lower temperatures when the density increases. In the present domain of investigation where the linear-response treatment of the ion-electron interaction is not suitable, the excess free energy cannot be separated as in Eq. (13).

Consequently, we have fitted the *ab initio* data by a functional form for the whole excess free energy, which still keeps the DWSC form but implicitly contains all the interactions between the species. The departure from a real one component plasma (OCP) model is in the dependence of the coefficients on the density, considered here as adjustable parameters. The F_{ex} form adjusted for the *ab initio* data in the fully dissociated fluid is

$$\begin{aligned} F_{ex}(\rho,T) &= Nk_BTa(\rho)\Gamma \\ &\quad + Nk_BT\left\{\frac{b(\rho)}{s}\Gamma^s + c(\rho)\,\ln(\Gamma) + d(\rho)\right\} \\ &\quad + \delta F_{ee}(\rho,T). \end{aligned} \tag{14}$$

This expression represents the free energy of an atomic partially ionized fluid. Its first line contains all the 0-K contributions. The second line represents the thermal ionic contributions, including *e-e* and *e-i* interactions. The third line is the thermal electronic contribution given in the IIT model [$\delta F_{ee}(\rho,T) = F_{ee}(\rho,T) - F_{ee}(\rho,0)$]. This expression of $\delta F_{ee}(\rho,T)$ was chosen as it is the dominant contribution at high temperature, thus, recovering the results of Chabrier and Potekhin's model in this limit. It is important to point out that the quality of the fit for the *ab initio* internal energy should guarantee that we have a good description of the free energy of the system. This is because the excess internal energy, given by a functional form of Γ and ρ, uniquely determines the free energy, F_{ex}, of the plasma through

$$f_{ex}(\Gamma,\rho) = \int_0^{\Gamma} \frac{u_{ex}(\Gamma',\rho)}{\Gamma'}\,d\Gamma', \tag{15}$$

where $f_{ex} = F_{ex}/Nk_BT$ and $u_{ex} = E_{ex}/Nk_BT$ are dimensionless quantities.

The free-energy form given by Eq. (14) does not account for the formation of H_2 molecules. A functional form that reproduces the free energy of the molecular fluid as well as the dissociating molecular fluid would be too complex to build. Consequently, we describe the dissociating molecular hydrogen fluid with a simple chemical equilibrium between a molecular and an atomic fluid for which the free energy is given by Eqs. (12) and (14). We relate the free energy of this fluid to the molecular fluid free energy through the mass action law under the assumption of a linear mixing of the molecular and the atomic species. The mass action law then gives

$$\frac{q_a^2}{q_m} = \frac{N_a^2}{N_m} = \frac{2N\alpha^2}{1-\alpha}, \tag{16}$$

where N is the total number of H atoms, q_a and q_m, respectively, are the atomic and molecular partitional functions [with the usual relation $F = -K_BT\,\ln(q)$] and α is the dissociation fraction. q_a is explicitly given by the free energy from Eqs. (12) and (14). Using Eq. (16), we can write the total free energy for a partially dissociated liquid as

$$\begin{aligned} F(\rho,T) &= F_{id}^{(i)} + F_{id}^{(e)} \\ &\quad + Nk_BT\left\{a(\rho)\Gamma + \frac{b(\rho)}{s}\Gamma^s + c(\rho)\ln(\Gamma) + d(\rho)\right\} \\ &\quad + \delta F_{ee}(\rho,T) + Nk_BT\left\{\ln\alpha + \frac{1-\alpha}{2}\right\}. \end{aligned} \tag{17}$$

The dissociation fraction α is used as an adjustable function of density and temperature. We assume that the degree of dissociation can be described by a Fermi function. This form was used to fit the dissociation fraction extracted from the QMD simulations by Holst *et al.*[23] So α is given by

$$\alpha(\rho,T) = \frac{1}{e^{[B(\rho)/T - C(\rho)T]} + 1}, \tag{18}$$

where $B(\rho)$ and $C(\rho)$ are two adjustable functions. An interesting property of this Fermi function is its limit at $T = 0$ K (hence, for a fraction of dissociation going to 0),

$$\lim_{T\to 0}\left(k_BT\left\{\ln\alpha + \frac{1-\alpha}{2}\right\}\right) = -k_BB(\rho), \tag{19}$$

which corrects the atomic free energy to give the molecular free energy. As shown in Sec. IV, this provides a very satisfactory representation of the free energy of the molecular fluid.

From the free energy expression given by Eq. (17), the expression for the internal energy $E = F - T(\frac{\partial F}{\partial T})_\rho$ and the pressure $P = \rho^2(\frac{\partial F}{\partial \rho})_T$ are straightforwardly obtained. These two expressions are used to adjust the a, b, c, d, B, and C density functions and the parameter s to reproduce the QMD and PIMC results [see Eqs. (20)–(30)]. The hydrogen density

ρ is expressed in g/cc (for another isotope: $\rho = \frac{m_H}{m_{\text{isotp}}}\rho_{\text{isotp}}$) and $\Gamma = 2.268\,79 \times 10^5 \rho^{1/3}/T$ (K),

$$a(\rho) = -0.731\,807 + (-3.084e-3)\rho + 0.352\,77\,\ln(\rho) + (8.8546e-3)[\ln(\rho)]^2 + 0.014\,805\,267[\ln(\rho)]^3, \quad (20)$$

$$b = 0.275\,457\,265, \quad (21)$$

$$c = -0.320\,95, \quad (22)$$

$$s = 0.321\,308, \quad (23)$$

$$d(\rho) = d_0 + \frac{32.1514}{16.3339}\exp(-16.3339\rho) + d_c(\rho), \quad (24)$$

$$d_0 = -0.274\,3876, \quad (25)$$

if $\rho \leqslant 0.337$,

$$d_c(\rho) = -0.163\,699\,29\rho, \quad (26)$$

if $0.337 \leqslant \rho \leqslant 0.419$,

$$d_c(\rho) = -0.163\,699\,29\rho + 2.394\,940\,122\rho\left(\frac{\rho}{2} - 0.337\right), \quad (27)$$

if $0.419 \leqslant \rho$,

$$d_c(\rho) = 0.032\,6858\rho, \quad (28)$$

$$B(\rho) = \exp(9.148\,95 - 2.069\,13\rho), \quad (29)$$

$$C(\rho) = \exp(-8.6253 + 2.8804\rho). \quad (30)$$

The constant d_0 is computed to obtain the same free energy of hydrogen in the dissociated regime as the one computed by Morales *et al.*[24]

We can see both in Fig. 6 and in Fig. 7 that our parametrization of the free energy reproduces the QMD and CEIMC calculations at low temperature and the PIMC at higher temperature. The accuracy of our fit is better than 2% over the whole density range and for temperatures up to 2 eV (that covers the conditions of the interior of giant planets). The worst accuracy (≈5%) is obtained when we extend the QMD calculations by the PIMC calculations, specifically for temperatures in a range of 5–7 eV.

Finally, in Fig. 8, it is interesting to compare the effective dissociation fraction obtained through the fit of the QMD thermodynamical quantities using Eq. (17) with the microscopic dissociation fractions that can directly be computed. Holst *et al.*[23] have used two criteria to estimate the fraction of H_2 molecules in their QMD simulation. In the first criterion, the number of molecules is calculated by counting the number of atoms located within a radius r_{bond} and which last for a time greater than ten vibrational periods. The second criterion uses values of the coordination number $K(r) = \frac{N-1}{V}\int_0^r 4\pi r'^2 g(r')\,dr'$, which is a weighted integral over the correlation function, $g(r)$, calculated in a supercell of volume V and containing N atoms. The microscopic dissociation fraction is plotted in Fig. 8, and it is compared to the estimation of the effective thermodynamical dissociation fraction of our model. They follow a similar trend with temperature at a given density. Our model identifies a similar transition from the molecular fluid to the fully atomic state as given by the microscopic output of the simulations. In particular, we see that the molecular to atomic transition is getting more abrupt as the density increases. But we should again stress that, although this dissociation fraction may carry some microscopic physical meaning, it formally remains an adjustable parameter that compensates for drastic approximations of our model of free energy, such as the linear mixing approximation and the simple chemical evolution of fluid hydrogen.

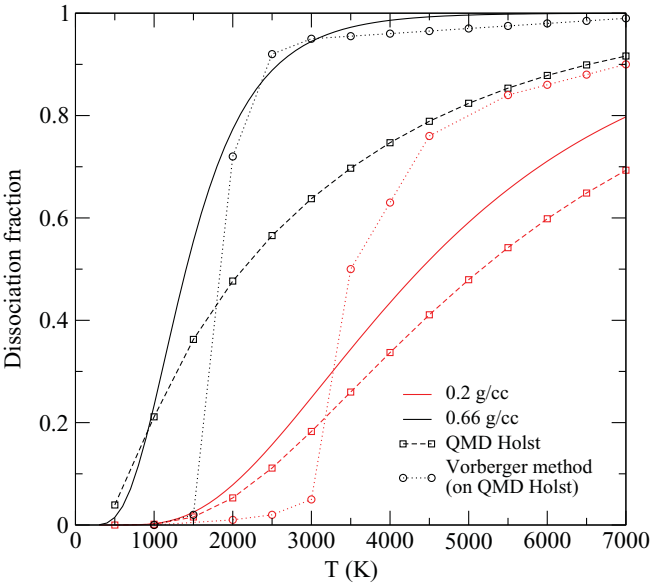

FIG. 8. (Color online) Dissociation fraction versus temperature. The fitted parameter α is compared to the microscopic quantity, as obtained by Holst *et al.*[23] using two microscopic criteria.

B. Quantum corrections to classical ionic behavior

In the QMD simulations, the ions are described classically. The quantum contribution associated with the ionic motion of the proton are not negligible in dense hydrogen fluid in the 1000-K range in both the molecular and the atomic states. Thus, it is important to take into account this quantum correction to bring the present fluid EoS to the same level as the EoS obtained in the solid phase. A well-known approach to estimate the first-order quantum correction from a classical simulation is to use the Wigner[56] and Kirkwood[57] $\hbar^2$ development of the free energy. The quantum correction is then expressed as

$$F_q = \frac{1}{24}N\hbar^2(k_B T)^2\langle f_i^2\rangle/m. \quad (31)$$

However, in order to match the present functional form of the fluid free energy, it was more convenient to estimate the ionic quantum correction differently. Following Eq. (17), $F^{\text{qc}}(\rho,T)$ is expressed as

$$F^{\text{qc}}(\rho,T) = F_a^{\text{qc}}(\rho,T) - k_B T\left\{\frac{\alpha^q - \alpha^c}{2} - \ln\left(\frac{\alpha^q}{\alpha^c}\right)\right\}, \quad (32)$$

where $F_a^{\rm qc}(\rho,T)$ is the ionic quantum correction in a fully dissociated fluid and α^q and α^c, respectively, are the effective dissociation fraction when ionic quantum corrections are taken into account or not. $F_a^{\rm qc}(\rho,T)$ is expressed as the quantum correction of a three-dimensional Einstein oscillator associated with the effective average motion of the proton. $\Theta_E(\rho)$ being the temperature of this oscillator, the quantum correction to the atomic partition function is given by

$$q_a^{\rm qc} = \left(\frac{\exp\left[-\Theta_E(\rho)/2T\right]}{1-\exp\left[-\Theta_E(\rho)/T\right]}\frac{\Theta_E(\rho)}{T}\right)^3, \tag{33}$$

and

$$F_a^{\rm qc}(\rho,T) = -K_B T \ln\left(q_a^{\rm qc}\right). \tag{34}$$

The effective Einstein frequency associated with the proton motion can be computed directly in the QMD simulation following the method proposed by Berens *et al.*[58] to calculate the ionic quantum correction in water. It is obtained from the ratio of the average of the square of the force on the protons over the average of the square of their velocity, as

$$\Theta_E^2(\rho) = \frac{\langle f_i^2\rangle}{m^2\langle v_i^2\rangle}\frac{\hbar}{k_B}. \tag{35}$$

Over the density range of the present simulations, $\Theta_E(\rho)$ (in K) is well reproduced by the following linear fit:

$$\Theta_E(\rho) = 452.79 + 390.49\rho. \tag{36}$$

If we assume that the main zero-point ionic contribution in the molecular phase is due to the vibron mode, the quantum correction to the molecular partition function can then be written as

$$q_m^{\rm qc} = \frac{\exp\left(-\Theta_{\rm vib}/2T\right)}{1-\exp\left(-\Theta_{\rm vib}/T\right)}\frac{\Theta_{\rm vib}}{T}. \tag{37}$$

Neglecting the temperature and density variation of the vibron, $\nu_{\rm H_2} \approx 4155.2\ {\rm cm}^{-1}$ and $\nu_{\rm D_2} = \sqrt{2}\nu_{\rm H_2}$, we can rewrite the mass action law as

$$\frac{\left(q_a^c q_a^{\rm qc}\right)^2}{q_m^c q_m^{\rm qc}} = \frac{N_a^2}{N_m} = \frac{2N(\alpha^q)^2}{1-\alpha^q}, \tag{38}$$

where q_a^c and q_m^c are the classical partition functions of the atomic and molecular fluids. By combining Eqs. (16) and (38), α^q, the dissociation fraction when the ionic quantum corrections are taken into account, can straightforwardly be related to the dissociation fraction obtained for classical protons and to $q_a^{\rm qc}$ and $q_m^{\rm qc}$ by

$$\frac{(\alpha^q)^2}{1-\alpha^q} = \frac{(\alpha^c)^2}{1-\alpha^c}\frac{\left(q_a^{\rm qc}\right)^2}{q_m^{\rm qc}}. \tag{39}$$

We check that this alternative estimation of the quantum ionic contribution to the free energy as given by Eq. (32) is in very good agreement with the one directly computed with the Wigner-Kirkwood formula given in Eq. (31). In Fig. 9, we plotted the temperature evolution of the effective dissociation fraction, α^q, at three densities and compared it to its classical estimation. Following the preceding observation that the effective dissociation parameter of the model follows a similar trend as the real microscopic dissociation parameter,

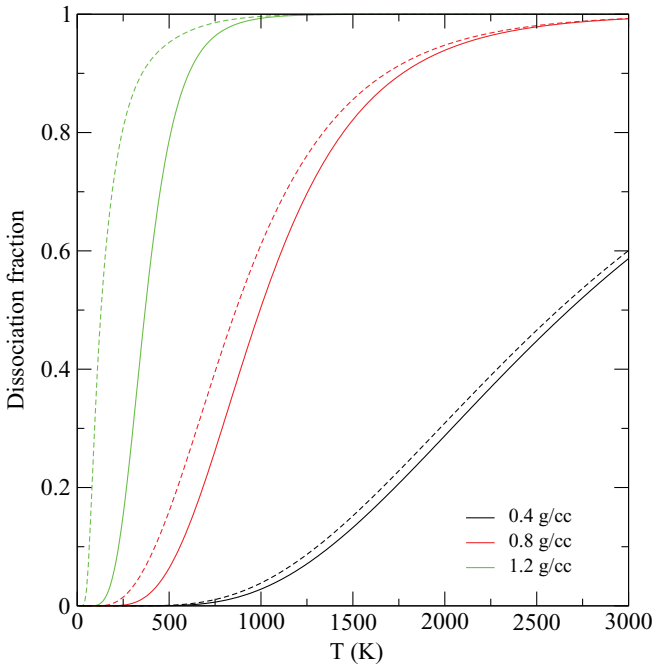

FIG. 9. (Color online) Influence of the quantum corrections on the dissociation fraction for three densities; the classical dissociation fractions as a solid line and the dissociation fractions with quantum corrections as a dashed line.

we can infer that the ZPM correction favors the dissociation of the H_2 molecules. This effect becomes stronger when the density increases. In fact, it can be intuitively explained by the gain of zero-point energy when a molecule dissociates.

IV. COMPARISON WITH EXPERIMENTAL DATA

In Secs. II–IV, we described how two forms of the free energy, one for the solid and one for the fluid, can reproduce the *ab intio* electronic structure calculations. We stress that no experimental data have been used to fit the parameters of the free-energy forms. The comparison of the present *ab initio* EoS with experiments should now be made to test its accuracy. It should be stressed that since the level of approximation of the *ab initio* calculations applies almost evenly over the thermodynamic domain investigated, the validation of the accuracy of the EoS over a small experimental domain should bring some confidence for similar accuracy over the full domain of investigation. Consequently, in this section, we will compare the output of the present EoS to the main thermodynamic measurements available on hydrogen at high pressure. These are the following: the determination of the solid EoS at 300 K, the sound velocity measurements in the molecular fluid, the Hugoniot curves of cryodeuterium and cryohydrogen, and the melting line of hydrogen. The comparison is very satisfactory, and it is made in the region where the properties should be less accurately captured by DFT due to the known dispersion forces or gap problems. The comparison with the 300-K solid EoS has been discussed already in Sec. II since it has been used to select the GGA approximation for the exchange-correlation functional.

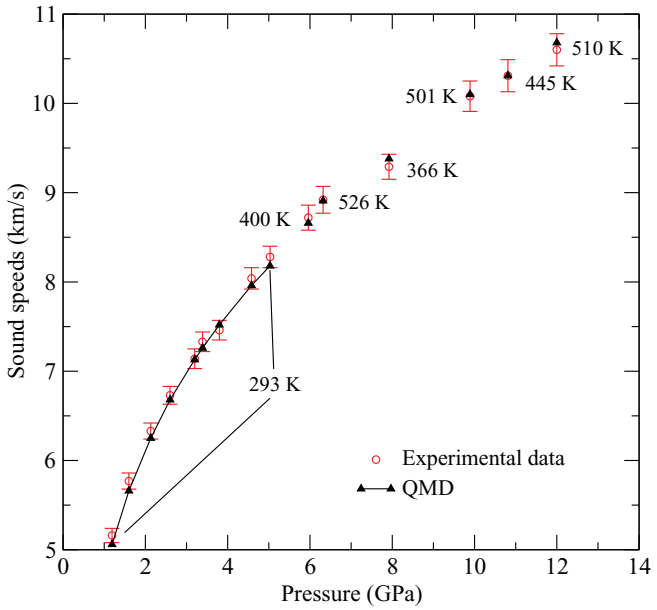

FIG. 10. (Color online) Adiabatic sound velocity of fluid H_2 versus pressure at various temperatures. The experimental points of Ref. 59, plotted as red dots with associated error bars, are compared to the calculated values for the same P and T.

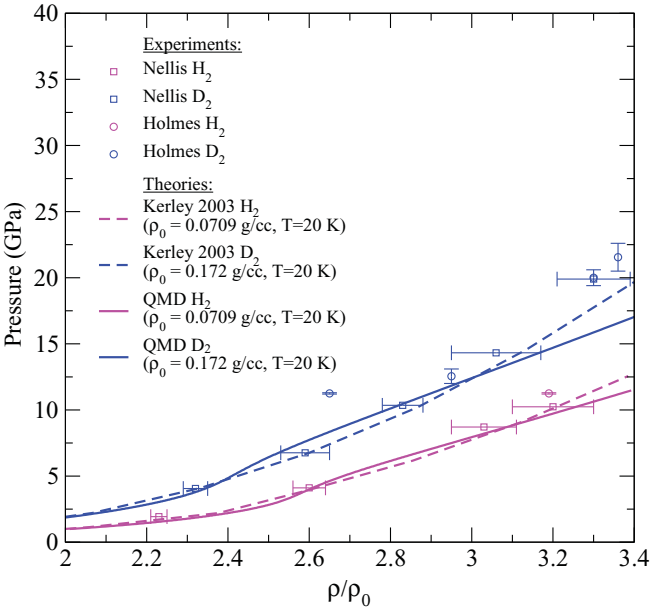

FIG. 11. (Color online) Principal Hugoniot curve of H_2 and of D_2 in the molecular fluid domain. The pressure is plotted versus the compression ratio. The prediction of the present EoS, as a full line, is compared to the experimental data.[5,60] The dashed line is the SESAME EoS.[1]

A. Sound velocity in the dense molecular fluid

From Eq. (17), the molecular free energy is obtained in the limit where the fraction of dissociation tends to 0. This description of the fluid molecular free energy is tested on the Brillouin scattering measurements of the sound velocity of fluid molecular hydrogen in the pressure range (1–12 GPa) and temperature (293–526 K).[59] The adiabatic sound velocity is calculated using the present EoS and the following formula:

$$c_u = \sqrt{\left(\frac{\partial P}{\partial \rho}\right)_s}. \tag{40}$$

Figure 10 shows that very good agreement is obtained between the calculated and experimental sound velocities.

B. Cryo-Hugoniot of H_2 and D_2

Dynamical measurements of the velocities in a planar shock experiment provide an absolute determination of the EoS data of a dense fluid. Specifically, the compression ratio versus pressure is generally the significant output. Planar shock measurements have been accurately made on cryotargets of D_2 and H_2 using a two-stage light gas gun.[5,60] In Fig. 11, these dynamic experimental data are compared to the Hugoniot curve calculated for H_2 and D_2 at the same initial density as the experimental one, using the present EoS and the SESAME EoS.[1] In this pressure range, both fluids are molecular, with a negligible dissociation fraction. Very good agreement between experimental data and the calculated Hugoniot is observed. The SESAME Hugoniot seems to fit the experimental data a little better. This should not be surprising since these experimental data have been used to fit this chemical model. The difference between the compression ratio of H_2 and of D_2 versus pressure along the Hugoniot appears because the initial density of cryo-H_2 and of cryo-D_2 is different. This difference reflects the effect of the initial density on the compression ratio along the Hugoniot rather than the isotopic shift between the EoS of H_2 and of D_2, which is much smaller.

Over the past ten years, the Hugoniot of cryo-D_2 has been extended up to about 200 GPa using various experimental approaches. The latest set of data points as obtained by laser-driven compression with the Nova laser[8,61] and the Omega laser[9] (possibly slightly shifted by a correction on the EoS of the quartz standard[10]) by explosive-driven compression[7,62,63] and by Z-pinch-driven compression[10] are compared in Figs. 12 and 13 to the calculated Hugoniot obtained with the present EoS. Above 20 GPa, the Hugoniot probes the evolution from a molecular fluid to a fully dissociated plasma. It is observed that the Hugoniot generated with the present EoS agrees very well with the body of experimental data, except for the NOVA data.[8,61] The predictions of various chemical models are also plotted for comparison, namely, the SESAME,[1] the Ross,[3] the Saumon-Chabrier-van Horn,[2] and the fluid variational theory (FVT)[64] ones. They generally tend to predict a too large maximum compression ratio at high pressure. The SESAME EoS that seems to be in better agreement tends more slowly toward the limit of compression of an ideal gas above 120 GPa. If all chemical models agree in the molecular fluid regime, they diverge in the domain of maximum compression. This reflects the difficulty of correctly describing the transition to the dense plasma state.

The principal Hugoniot of D_2 has been obtained previously by various *ab initio* calculations. As seen in Figs. 14 and 15, the present EoS is in good agreement with these previous calculations. Yet some differences exist that are essentially due to the form of the fit of the *ab initio* data and to the treatment of the quantum corrections. We believe that the present paper is an

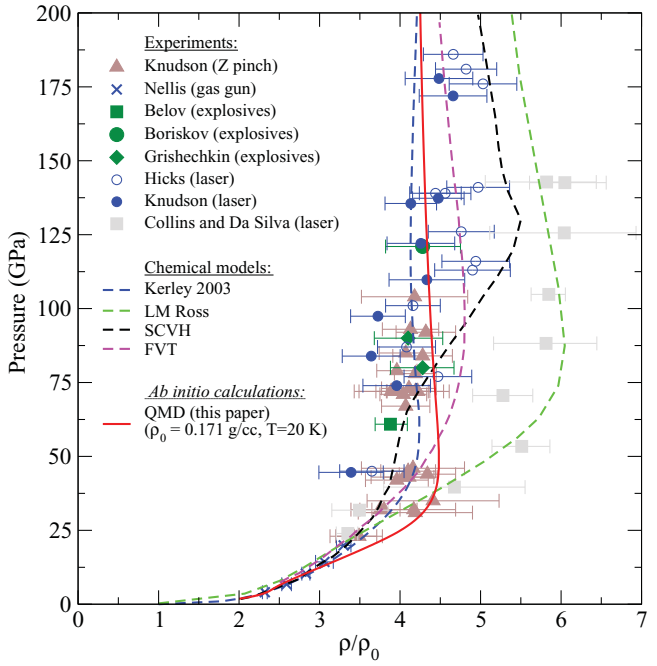

FIG. 12. (Color online) Comparison between the measured and some calculated principal Hugoniot for D_2 at high densities. The latest experimental data are plotted as symbols with error bars: Z machine (triangles[6]), gas gun (crosses[5]), explosives [green squares,[62] (larger) circles,[7] and diamonds[63]], and laser [open circles,[9] full (smaller) circles,[10] and gray squares[8,61]]. The present EoS calculation, as a full line, is compared to the predictions of various chemical models: Kerley,[1] Ross,[3] Saumon-Chabrier-van Horn,[2] and FVT.[64]

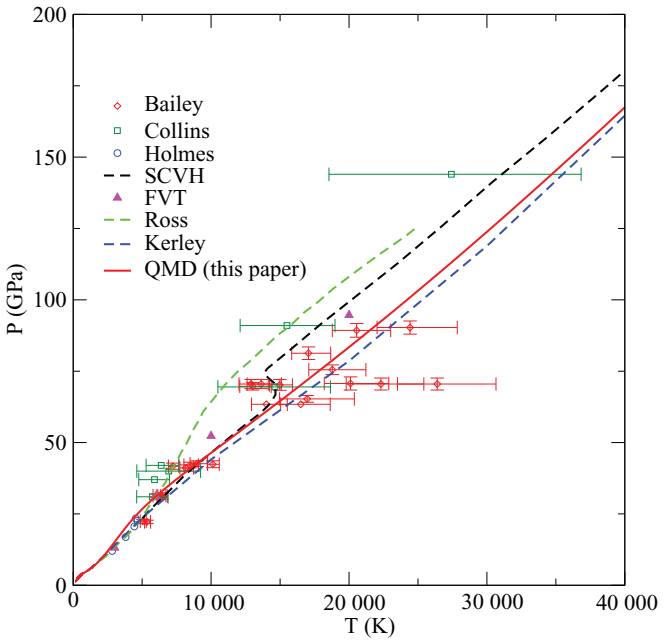

FIG. 13. (Color online) Comparison between the measured and some calculated principal Hugoniot for D_2 at high densities in the P-T diagram. The latest experimental data are plotted as symbols with error bars: Z machine (diamonds[66]), laser (green squares[48]), and gas gun (blue circles[60]). The present EoS calculation, as a full line, is compared to the predictions of various chemical models: Kerley,[1] Ross,[3] Saumon-Chabrier-van Horn,[2] and FVT.[64]

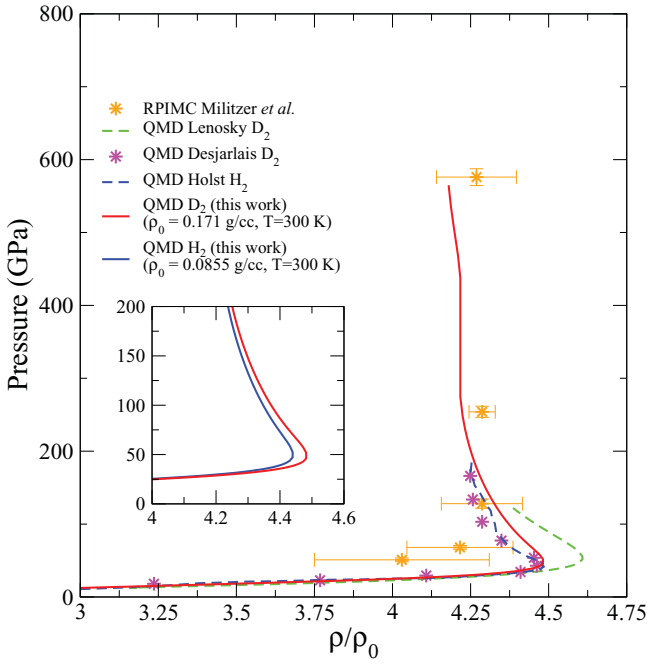

FIG. 14. (Color online) Comparison between different *ab initio* computations of the principal Hugoniot for D_2: present EoS, restricted path integral Monte Carlo (RPIMC),[19] and QMD.[17,21,23] Inset: The isotopic shift in the maximum compression rate along a Hugoniot starting at the same molar volume in D_2 and H_2 at 300 K.

improvement over the previous calculations concerning these two issues. Furthermore, the present free-energy model allows one to compute the isotopic shift on the EoS of dense fluid hydrogen. The influence of the ZPM on the principal Hugoniot of hydrogen in the region of its compression ratio maximum is plotted in the inset of Fig. 14. We generate the Hugoniot curve of H_2 and D_2, starting at the same molar volume and the same initial pressure (3 kbar) at 300 K. This is essentially what can be measured in a laser-shock compression on precompressed targets.[65] Here, a small isotopic shift is predicted, essentially due to the difference in the reference energy between the two isotopes.

C. Multiple-shock experiments

Numerous experiments have been carried out that explore the double- and multiple-shock properties of hydrogen. In ICF applications, the timing of multiple shocks is critical. However, we have not included the output of these experiments in the systematic test of the present EoS because their observables are not unambiguously nor simply related to the thermodynamical data of the EoS. In the case of the reshock experiments, the observables are based on the combination of the EoS of hydrogen and of the EoS of the anvil for the reshock (i.e., the EoS of quartz in the study of Boehly *et al.*[67] and the EoS of quartz, sapphire, and Al in the study of Knudson *et al.*[6]). In these experiments, the accuracy of the EoS of the anvil is also an important input. Similarly, the comparison of our EoS to the multishock experiments would require a specific explanation on the geometry of multiple shocks, which is beyond the scope of this paper.

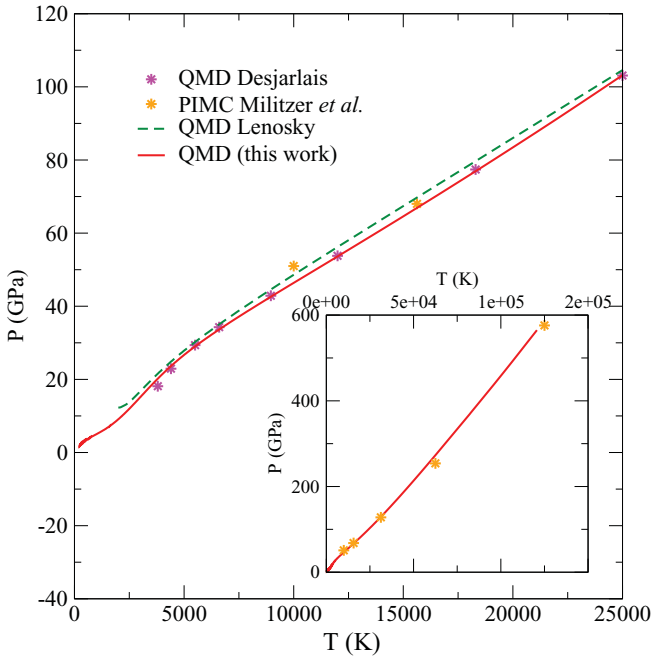

FIG. 15. (Color online) Comparison between different *ab initio* computations of the principal Hugoniot for D_2 in the P-T diagram: present EoS, RPIMC,[19] and QMD.[17,21,23] Inset: Comparison with RPIMC calculation up to 125 000 K.

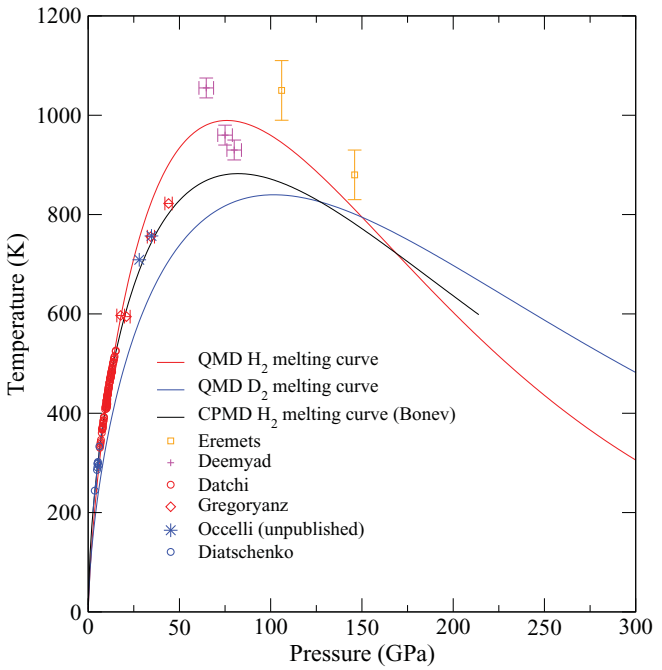

FIG. 16. (Color online) Melting curve of H_2 solid. The various symbols represent various experimental determinations.[69–72] The red (top) line is the present free-energy determination. The black (middle) line is the moving interface determination of Bonev *et al.*[22] The blue (bottom) line is the present free-energy determination of the D_2 melting.

D. Melting curve

The computation of the melting curve is known to be a sensitive test of the free-energy description of the solid and the liquid phases. Using the free-energy functionals of the solid and liquid states previously given, the melting curve of hydrogen can be calculated by equalizing the Gibb's free energies. The calculated melting curve obtained presents a maximum, and it is well parametrized using the functional form given by Kechin[68] as

$$T_m = T_0(1 + P/a)^b \exp(cP), \tag{41}$$

where T_m is in (K), $T_0 = 4.852\,66$, $a = 0.022\,8677$, $b = 0.747\,862$, and $c = 0.009\,826\,57$ for H_2. The extrapolation of the melting curve, obtained from measurements up to 20 GPa (Ref. 69) suggested that the melting curve of hydrogen could have a maximum at about 1100 K and 120 GPa. Subsequent measurements extended the melting curve of hydrogen to higher pressures and confirmed the existence of a maximum. These various experimental data[69–72] are compared to the present calculated melting curve in Fig. 16. The agreement is indeed very good with the calculated melting line, interpolating through the scatter of the various experimental measurements. It should be recalled that the measurements of the melting points of hydrogen above 500 K are challenging, and the accuracy of the experimental data is still being discussed.[73] The QMD calculation of the melting line has been performed by Bonev *et al.*[22] using the two phases simulation approach and the GGA approximation for the exchange-correlation function. With this method, melting was determined when the interface between an hcp solid and a fluid was seen to be stable during an isothermal-isobaric (NPT) simulation. Their calculation established the existence of a maximum on the high-pressure melting curve located at about 90 GPa and a temperature around 900 K. We compare these results to ours in Fig. 16, and we see that the melting curves are rather similar, with the most noticeable difference concerning the prediction of the maximum temperature reached. It is worth pointing out that, although both calculations are based on the QMD approach with the same exchange-correlation functional, there exist several differences between them that may explain this discrepancy. Specifically, the moving interface method may suffer from finite-size effects, which are hard to quantify but do not affect the free-energy results. Conversely, the free-energy method may suffer from uncertainty coming from the functional chosen for exchange and correlation effects. The molecular dynamics approach accounts for anharmonicity, while the free-energy formulation neglects this effect as it is based on a DFPT description of the solid phase. Finally, Bonev's calculations are classical simulations that do not take the ZPM into account. As will be seen in Sec. V, taking the ionic ZPM into account leads to a significant isotopic shift on the melting curve of hydrogen that is of similar magnitude to the difference between the present and Bonev's calculations.

V. TWO PREDICTIONS

A. Isotopic shift on the melting curve

The insertion of the ZPM contribution to the free energy of solid and fluid hydrogen, as described in Secs. II and III, allows one to address the question of the magnitude of the isotopic shift on the melting curve. The calculated melting

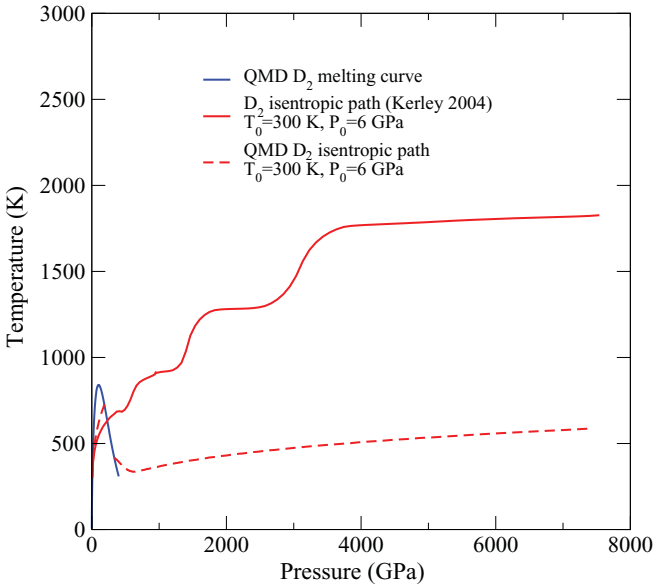

FIG. 17. (Color online) Isentropic compression trajectories in the liquid, using the initial conditions indicated in the figure and compared to the SESAME results.[1]

curve of deuterium is also well parametrized using the Kechin functional form with the following parameters: $T_0 = 10.529$, $a = 0.035\,0601$, $b = 0.647\,859$, and $c = 0.006\,5481$ for D_2. In Fig. 16, the D_2 melting curve is compared to the H_2 melting curve. A significant isotopic shift is observed, presenting an unexpected feature. At a given low pressure, the melting temperature of D_2 is lower than the melting temperature of H_2, in agreement with the original prediction using molecular pair interaction.[74] But above 120 GPa, the two melting curves cross, and solid D_2 melts at a higher temperature than solid H_2. This inversion of the quantum isotopic shift should be related to the change of nature of the molecular fluid that is dissociating. It should be noted that the magnitude of this isotopic shift is only semiquantitatively correct, especially on the molecular fluid side for which some contributions to the quantum correction have been discarded. The crossing of the two melting curves is certainly an intriguing prediction that should stimulate its experimental observation.

B. Isentropic compression path

Having a free-energy form of the EoS of hydrogen allows for the computation of compression paths for hydrogen, which can be very useful for designing dynamic experiments. As an example, in Fig. 17, we show an isentropic compression of deuterium starting from a solid state at 6 GPa and 300 K that goes to a density of 10 g/cc. The temperature along a given isentrope is obtained by using the following formula:

$$T = T_0 \exp\left[\int_{V_0}^{V} \left(\frac{\partial P}{\partial E}\right)_V dV\right], \tag{42}$$

where T_0 and V_0, respectively, are the initial temperature and the initial volume. As seen in Fig. 17, the calculated isentropic path in the P-T diagram is significantly different from the one calculated with the most advanced SESAME EoS.[1] A very interesting output of this calculation is that the temperature increase is quite modest. Hence, if a near-isentropic compression of hydrogen could be designed, a very interesting domain of the phase diagram of hydrogen would be probed. Also, a significant discontinuity is predicted at melting that should be observable.

VI. CONCLUSION

To summarize, we have built a multiphase EoS of hydrogen isotopes entirely from first-principle calculations. The ZPM of the nuclei is taken into account. It covers a large phase space of hydrogen, from the $T = 0$ K solid up to the dense plasma domain where established approximations are shown to be valid. A complete QMD data set has been constructed in the molecular solid phase. Some QMD data calculations have been performed in the fluid state to complete the extensive body of literature. Physical models fitted on these data allow one to obtain a description of the free energy. The accuracy of this EoS is tested on all the thermodynamic measurements of dense hydrogen available to date. The comparison is very satisfactory, and it is made in the region where the properties should be less accurately captured by DFT due to the known dispersion forces or gap problems. Also, because of the homogeneity of the approach over the whole phase space considered here, the experimental validation of the EoS over a restricted experimentally accessible domain should be extended with confidence to the untested domain. The present form of the EoS should make it easily usable by others. In particular, it should now be applied to important applications for which the domain of the hydrogen EoS covered here is a central input, such as ICF or planetary interiors. Also, we think that it should prove useful for designing dynamic compression measurements of hydrogen that are becoming feasible with the use of large laser facilities,[75] as illustrated by the significant effect shown on the calculation of an isentrope path. Finally, an interesting prediction of a measurable isotopic shift on the hydrogen melting curve is made that would be a definitive test of the present EoS.

[1] G. I. Kerley, Technical Report No. SAND2003-3613, Sandia National Laboratories, 2003 (unpublished).
[2] D. Saumon, G. Chabrier, and H. M. van Horn, Astrophys. J., Suppl. Ser. **99**, 713 (1995).
[3] M. Ross, Phys. Rev. B **58**, 669 (1998).
[4] P. Loubeyre, R. LeToullec, D. Hausermann, M. Hanfland, R. Hemley, H. k. Mao, and L. Finger, Nature(London) **383**, 702 (1996).
[5] W. J. Nellis, A. C. Mitchell, M. van Thiel, G. J. Devine, R. J. Trainor, and N. Brown, J. Chem. Phys. **79**, 1480 (1983).
[6] M. D. Knudson, D. L. Hanson, J. E. Bailey, C. A. Hall, J. R. Asay, and C. Deeney, Phys. Rev. B **69**, 144209 (2004).
[7] G. V. Boriskov, A. I. Bykov, R. I. Il'kaev, V. D. Selemir, G. V. Simakov, R. F. Trunin, V. D. Urlin, V. E. Fortov, and A. N. Shuikin, Dokl. Akad. Nauk **392**, 755 (2003) [Dokl. Phys. **48**, 553 (2003)].

[8]G. Collins, L. DaSilva, P. Celliers, D. Gold, M. Foord, R. Wallace, A. Ng, S. Weber, K. Budil, and R. Cauble, Science **281**, 1178 (1998).
[9]D. G. Hicks, T. R. Boehly, P. M. Celliers, J. H. Eggert, S. J. Moon, D. D. Meyerhofer, and G. W. Collins, Phys. Rev. B **79**, 014112 (2009).
[10]M. D. Knudson and M. P. Desjarlais, Phys. Rev. Lett. **103**, 225501 (2009).
[11]R. Martin, *Electronic Structure: Basic Theory and Practical Methods* (Cambridge University Press, Cambridge, UK, 2004).
[12]A. Dewaele, M. Torrent, P. Loubeyre, and M. Mezouar, Phys. Rev. B **78**, 104102 (2008).
[13]A. A. Correa, L. X. Benedict, D. A. Young, E. Schwegler, and S. A. Bonev, Phys. Rev. B **78**, 024101 (2008).
[14]D. M. Ceperley and B. J. Alder, Phys. Rev. B **36**, 2092 (1987).
[15]T. W. Barbee, A. Garcia, M. L. Cohen, and J. L. Martins, Phys. Rev. Lett. **62**, 1150 (1989).
[16]J. C. Pickard and R. J. Needs, Nat. Phys. **3**, 473 (2007).
[17]T. J. Lenosky, S. R. Bickham, J. D. Kress, and L. A. Collins, Phys. Rev. B **61**, 1 (2000).
[18]G. Galli, R. Q. Hood, A. U. Hazi, and F. Gygi, Phys. Rev. B **61**, 909 (2000).
[19]B. Militzer and D. M. Ceperley, Phys. Rev. Lett. **85**, 1890 (2000).
[20]S. Bagnier, P. Blottiau, and J. Clérouin, Phys. Rev. E **63**, 015301 (2000).
[21]M. P. Desjarlais, Phys. Rev. B **68**, 064204 (2003).
[22]S. A. Bonev, E. Schwegler, T. Ogitsu, and G. Galli, Nature (London) **431**, 669 2004.
[23]B. Holst, R. Redmer, and M. P. Desjarlais, Phys. Rev. B **77**, 184201 (2008).
[24]M. A. Morales, C. Pierleoni, and D. M. Ceperley, Phys. Rev. E **81**, 021202 (2010).
[25]B. Militzer, D. M. Ceperley, J. D. Kress, J. D. Johnson, L. A. Collins, and S. Mazevet, Phys. Rev. Lett. **87**, 275502 (2001).
[26]E. D. Chisolm, S. D. Crockett, and D. C. Wallace, Phys. Rev. B **68**, 104103 (2003).
[27]D. M. Ceperley, Rev. Mod. Phys. **67**, 279 (1995).
[28]V. P. Glazkov, S. P. Besedin, I. N. Goncharenko, A. V. Irodova, I. N. Makarenko, V. A. Somenkov, S. M. Stishov, and S. S. Shilsteyn, Pis'ma Zh. Eksp. Teor. Fiz. **47**, 661 (1988); JETP Lett. **47**, 661 (1988).
[29]A. F. Goncharov, I. I. Mazin, J. H. Eggert, R. J. Hemley, and H. K. Mao, Phys. Rev. Lett. **75**, 2514 (1995).
[30]I. Goncharenlo and P. Loubeyre, Nature (London) **435**, 1206 (2005).
[31]J. Kohanoff, S. Scandolo, G. L. Chiarotti, and E. Tosatti, Phys. Rev. Lett. **78**, 2783 (1997).
[32]K. Nagao and H. Nagara, Phys. Rev. Lett. **80**, 548 (1998).
[33]K. A. Johnson and N. W. Ashcroft, Nature (London) **403**, 632 (2000).
[34]M. Stadele and R. M. Martin, Phys. Rev. Lett. **84**, 6070 (2000).
[35]K. Nagao, T. Takezawa, and H. Nagara, Phys. Rev. B **59**, 13741 (1999).
[36]J. Van Kranendonk, *J. Solid Hydrogen: Theory of the Properties of Solid* H_2, *HD,* D_2 (Plenum, New York, 1983).
[37]ABINIT is a common project of the Universite Catholique de Louvain (Louvain-la Neuve, Belgium), Corning Incorporated, and other contributors.
[38]N. Troullier and J. L. Martins, Phys. Rev. B **43**, (1993).
[39]J. P. Perdew, K. Burke, and M. Ernzerhof, Phys. Rev. Lett. **77**, 3865 (1996).
[40]D. M. Ceperley and B. J. Alder, Phys. Rev. Lett. **45**, 566 (1980), parametrized in J. P. Perdew and A. Zunger, Phys. Rev. B **23**, 5048 (1981).
[41]P. Vinet, J. H. Rose, J. Ferrante, and J. R. Smith, J. Phys. C **1**, 1941 (1989).
[42]S. Ishmaev, I. Sadikov, A. Chernyskov, B. Vindryaevskii, A. Sukhoparov, A. Telepnev, and G. Kobelev, Sov. Phys. JETP **57**, 228 (1983).
[43]S. Ishmaev, I. Sadikov, A. Chernyskov, B. Vindryaevskii, A. Sukhoparov, A. Telepnev, G. Kobelev, and R. Dadykov, Sov. Phys. JETP **62**, 721 (1985).
[44]S. Baroni, S. de Gironcoli, A. Dal Corso, and P. Giannozzi, Rev. Mod. Phys. **73**, 515 (2001).
[45]L. J. Zhang, Y. L. Niu, T. Cui, Y. Li, Y. Wang, Y. M. Ma, Z. He, and G. T. Zou, J. Phys. Condens. Matter **18**, 9917 (2006).
[46]D. C. Wallace (Dover, New York, 1998).
[47]P. Loubeyre, F. Occelli, and R. LeToullec, Nature (London) **416**, 613 (2002).
[48]L. A. Collins, S. R. Bickham, J. D. Kress, S. Mazevet, T. J. Lenosky, N. J. Troullier, and W. Windl, Phys. Rev. B **63**, 184110 (2001).
[49]G. Chabrier and A. Y. Potekhin, Phys. Rev. E **58**, 4941 (1998).
[50]S. Galam and J. P. Hansen, Phys. Rev. A **14**, 816 (1976).
[51]H. A. DeWitt, W. Slattery, and G. Chabrier, Physica B **228**, 158 (1996).
[52]S. Ichimaru, H. Iyetomi, and S. Tanaka, Phys. Rep. **149**, 91 (1987).
[53]J. Kohanoff and J. P. Hansen, Phys. Rev. E **54**, 768 (1996).
[54]G. Chabrier, J. Phys. (Paris) **51**, 1607 (1990).
[55]A. Y. Potekhin and G. Chabrier, Contrib. Plasmas Phys. **50**, 82 (2010).
[56]E. Wigner, Phys. Rev. **40**, 749 (1932).
[57]J. Kirkwood, Phys. Rev. **44**, 31 (1933).
[58]P. H. Berens, D. H. J. Mackay, G. M. White, and K. R. Wilson, J. Chem. Phys. **79**, 2375 (1983).
[59]K. Matsuishi, E. Gregoryanz, H. k. Mao, and R. Hemley, J. Chem. Phys. **118**, 10683 (2003).
[60]N. C. Holmes, M. Ross, and W. J. Nellis, Phys. Rev. B **52**, 15835 (1995).
[61]L. B. Da Silva, P. Celliers, G. W. Collins, K. S. Budil, N. C. Holmes, T. W. Barbee Jr., B. A. Hammel, J. D. Kilkenny, R. J. Wallace, M. Ross, R. Cauble, A. Ng, and G. L. B. Chiu, Phys. Rev. Lett. **78**, 483 (1997).
[62]S. I. Belov and G. V. Boriskov, and A. I. Bykov *et al.*, JETP. Lett. **76**, 433 (2002).
[63]S. K. Grishechkin, S. K. Gruzdev, V. K. Gryaznov, M. V. Zhernokletov, R. I. Il'kaev, I. L. Iosilevskii, G. N. Kashintseva, S. I. Kirshanov, S. F. Manachkin, and V. B. Mintsev *et al.*, JETP Lett. **80**, 398 (2004).
[64]H. Juranek and R. Redmer, J. Chem. Phys. **112**, 3780 (2000).
[65]P. Loubeyre *et al.*, High Press. Res. **24**, 25 (2004).
[66]J. E. Bailey, M. D. Knudson, A. L. Carlson, G. S. Dunham, M. P. Desjarlais, D. L. Hanson, and J. R. Asay, Phys. Rev. B **78**, 144107 (2008).
[67]T. R. Boehly *et al.*, Phys. Plasmas **11**, L49 (2004).
[68]V. Kechin, J. Phys. Condens. Matter **7**, 531 (1995).
[69]F. Datchi, P. Loubeyre, and R. LeToullec, Phys. Rev. B **61**, 6535 (2000).

[70]E. Gregoryanz, A. F. Goncharov, K. Matsuishi, H. K. Mao, and R. J. Hemley, Phys. Rev. Lett. **90**, 175701 (2003).
[71]S. Deemyad and I. F. Silvera, Phys. Rev. Lett. **100**, 155701 (2008).
[72]M. I. Eremets and I. A. Trojan, Pis'ma. v. ZhETF **89**, 198 (2009).
[73]A. Goncharov, R. J. Hemley, and E. Gregoryanz, Phys. Rev. Lett. **102**, 149601 (2009).
[74]P. Loubeyre and J. P. Hansen, Phys. Lett. **80**, 181 (1980).
[75]R. Jeanloz, P. Celliers, J. Eggert, K. Lee, S. McWilliams, S. Brygoo, and P. Loubeyre, Proc. Natl. Acad. Sci. USA **104**, 9172 (2007).